Available online at www.sciencedirect.com
SCIENCE DIRECT®
Journal of Chromatography A, 1027 (2004) 237–244
JOURNAL OF CHROMATOGRAPHY A
www.elsevier.com/locate/chroma

Parametric investigation on the effect of channel topologies on electrophoretic separations

David S.W. Lim, Jason S. Kuo, Daniel T. Chiu*

Department of Chemistry, University of Washington, Seattle, WA 98195-1700, USA

Abstract

This paper presents a systematic study that illustrates the importance of the topologies of microchannels on electrokinetically based separation. Using theoretical and numerical analyses, we designed and showed that topologies that significantly increased the surface-to-volume ratio of the channel can provide dramatic improvement in the ability of the channel both to dissipate the heat generated by Joule heating and to reduce the axial dispersion associated with the siphoning effect. The incremental benefit and tradeoff of geometric complexity was also evaluated. The improvement offered by topographically patterned channels, such as finned structures, is especially pertinent in the development of preparative or semi-preparative scale electrokinetically driven separations, such as capillary electrophoresis and capillary electrochromatography, in which large cross sections of channels are required to achieve the needed volumetric throughput.

Keywords: Capillary electrophoresis; Instrumentation; Microchannel topologies

1. Introduction

With advances in genomics and proteomics, there is an intense effort to understand the biochemical and biophysical functions of proteins and to use proteins as therapeutics. A prerequisite in many of these studies is the availability of proteins of high purity and concentration. Given that a typical cell lysate can consist up to ~20,000 proteins [1] spanning five orders of magnitude in abundance [2], the ability to isolate usable quantities of proteins from cells or extracts is crucial to protein structure characterization as well as to the clinical usages of proteins. In X-ray crystallography, for example, folded homogeneous proteins at concentrations in milligram per milliliter (mg/ml) typically are needed, and similar requirements exist for NMR analysis. A high resolution, preparative-scale separation system that is capable of addressing this formidable challenge will greatly facilitate these studies.

Protein purification can be performed with a number of techniques in chromatography, including high-performance liquid chromatography (HPLC) [3–5], ion-exchange chromatography [6], and affinity chromatography [6], as well as non-chromatographic methods, such as gel electrophoresis [7], gel filtration [8–10], and immunoprecipitation [11]. Of these methods, the high-resolution separation and purification of proteins at a preparative or semi-preparative scale has often been performed with HPLC owing to its ability to handle and separate complex mixtures of proteins and cell lysates. Despite its high separation efficiency, HPLC suffers from an intrinsic axial dispersion due to the parabolic velocity profile of pressure-driven flow [12]. It is the ability to overcome this axial dispersion in electroosmotic flow (EOF) that makes capillary electrophoresis (CE) and capillary electrochromatography (CEC) [12–14] highly efficient alternatives to HPLC for the analysis of small sample volumes.

Although CE has been in development since the 1970s and has been a subject of intense research activities throughout the past two decades, CE is used primarily at the analytical scale rather than at the preparative scale [15]. Two factors limit CE to small, nanoliter volumes of samples: (1) Joule heating, and (2) siphoning.

As the diameter increases in a conventional circular fused silica capillary, Joule heating becomes more prominent. There are two detrimental effects that arise from this heating: (1) the radial temperature profile in the capillary leads to a radial profile in solution viscosity, which in turn results in a parabolic velocity profile that causes axial dispersion

* Corresponding author.
E-mail address: chiu@chem.washington.edu (D.T. Chiu).

0021-9673/$ – see front matter © 2003 Elsevier B.V. All rights reserved.
doi:10.1016/j.chroma.2003.09.019

and degrades separation efficiency [16], and (2) the overall average temperature inside the capillary increases, which results in the formation of bubbles and the denaturation of proteins. Consequently, Joule heating must be properly dissipated to successfully scale up CE for preparative scale operations. Efforts to address this issue include the use of concentric capillaries [17] and non-aqueous buffers with low conductance [18].

In addition to these issues with thermal management, hydrodynamic consideration with EOF is another important factor in determining the resolution achieved by CE [15,19,20]. A recent study suggested that induced pressure gradient could produce significant axial dispersion inside a capillary [21,22], and flow instability has been observed recently in a preparative scale separation caused by electroosmotic disturbance [23]. In the capillary format, the fluidic resistance to siphoning is dramatically reduced as the diameter of the capillary increases, because of the familiar dependence of volumetric throughput on the fourth power of the radius of the capillary in Poisseuille flow. This lack of fluidic resistance in wide-bore capillaries (e.g., 200 μm) that causes siphoning is a major impediment to the use of CE in preparative scale separations. Although this siphoning is present in CE, it is nicely circumvented in other modes of separation in which the capillary is packed with a matrix, such as in CEC and capillary-gel electrophoresis (CGE). This fact has permitted the semi-preparative CEC to be developed and demonstrated by Chen et al. [24].

To overcome both the challenges posed by Joule heating and siphoning in scaling up CE to the preparative scale, we have examined the possibility of varying the topologies of the microchannels as a general strategy to improve heat dissipation and to eliminate siphoning in preparative scale CE. This paper presents a parametric study based on theoretical and numerical calculations on how the topologies of the microchannels affect heat transfer and siphoning in channels with large cross sections.

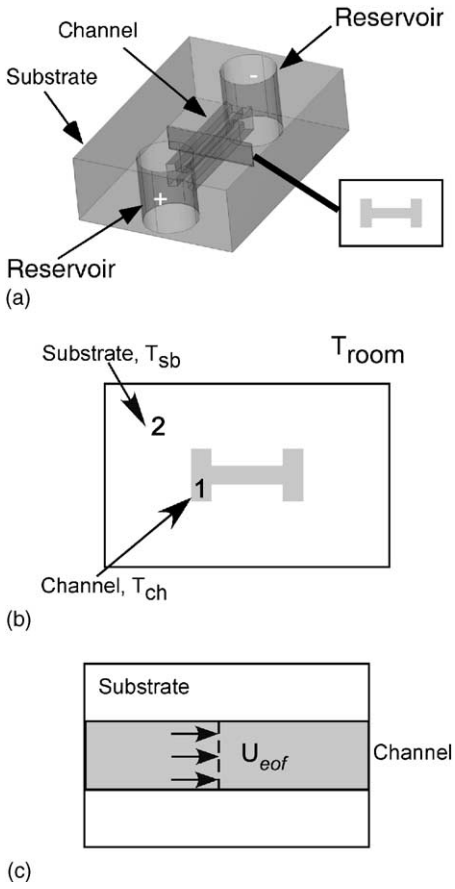

Fig. 1. Schematic showing the topographically patterned channels we studied: (a) layout of the design; the inset shows the cross section of a 4-fin channel, (b) cross-sectional schematic illustrating the heat transfer problem in a 4-fin channel, (c) side view showing the hydrodynamic problem. Note the schematics are not drawn to scale for ease of visualization.

2. Theory

Because the principal issues hindering the scale-up of capillary electrophoresis are (1) heat generation, and (2) susceptibility to hydrodynamic flow in large channels, we propose to address these issues by optimizing the channel geometry to increase the surface-to-volume ratio of the channel. Increasing surface-to-volume ratio provides larger interfacial area for heat transfer into the substrate. From a hydrodynamic perspective, larger surface-to-volume ratio also provides more no-slip boundary area to damp out any inadvertent pressure-driven flow, which can easily distort or overwhelm the electrokinetically driven flow. Fig. 1a shows a schematic of the proposed capillary system, which consists of the anode and cathode reservoirs and the main channel where the separation occurs. For clarity, the injection channel and the associated reservoirs have been omitted from the drawing. The cross-sectional geometry of the main channel is modified to increase the surface-to-volume ratio and one case studied in this paper is shown in the inset (a 4-fin structure).

In typical microfluidic systems where the main transport mode is electrokinetically driven (i.e., velocity < 1 cm/s, and $Re \leq 1$), MacInnes [25] has argued based on order of magnitude analysis that convective heat transport is negligible if $\xi^2\kappa^2 \gg PrRe_\zeta$, where ξ is the characteristic dimension of the channel, κ^{-1} is the thickness of the double layer, Pr (Prantl number) is defined as $\mu C_p/k$ (μ represents viscosity in Pa s, C_p is heat capacity at constant pressure in kJ/kg K, and k is the thermal conductivity in W/m K), and Re_ζ indicates Reynolds number calculated by using ξ as the length scale. With ξ being 500 μm in our microchannel and κ^{-1} being 20 nm, $\xi^2\kappa^2$ is 7×10^8 and $PrRe_\zeta$ is ~3 ($Pr \sim 3$ for water). The length scale of our microchannel is therefore too large for significant convective heat transfer. By neglecting the contribution of convective heat transfer, heat and momentum transport can be de-coupled in our calculations and the analysis is simplified tremendously.

The heat transport problem is illustrated in Fig. 1b with two main regions of consideration: (1) buffer region inside the channel where Joule heating is generated from the applied voltage [26,27], and (2) substrate region where thermal conduction occurs in the substrate material. Note that in region (1), thermal conduction also occurs in the buffer solution. Thus, the steady state energy transport can be described by:

$$-\nabla(k_i \nabla T) = Q$$
$$Q = \begin{cases} \sigma E^2 & \text{in } \Omega_1 \\ 0 & \text{in } \Omega_2 \end{cases} \quad (1)$$

where T is the temperature in Kelvin, k_i is the thermal conductivity with index i denoting the region of concern, Q is the volumetric heating rate in W/m^3, σ is the ionic conductivity of the buffer in S/m, E is the applied electric field, and Ω_1 and Ω_2 indicate region (1) and region (2), respectively. The physically plausible boundary conditions require that: (1) heat flux leaving buffer solution must equal to that entering the substrate, (2) temperature of the buffer solution must equal to that of the substrate at the interface, and (3) the temperature at the outer edge of the substrate is the same as the ambient temperature. This last condition is valid for most microfluidic devices constructed on a planar substrate because the dimensions of the substrate material are much larger than that of the channel and natural convection is negligible. Mathematically the boundary conditions can be written as:

$$\begin{aligned} k_1 \nabla T|_1 &= k_2 \nabla T|_2 \quad \text{at } \partial\Omega_1 \\ T|_1 &= T_2 \quad \text{at } \partial\Omega_1 \\ T &= T_{\text{ambient}} \quad \text{at } \partial\Omega_2 \end{aligned} \quad (2)$$

To satisfy the last boundary condition, the cross-sectional dimension of the substrate is set to at least 1 cm × 1 cm in our numeric calculations.

Joule heating, or heat generation as a result of current conduction in ionic solution, is a strong function of temperature. This dependence can be modeled by introducing temperature-dependent buffer ion conductivity [28]:

$$\sigma = \sigma_0[1 + \alpha(T - T_0)], \quad (3)$$

where σ_0 is the reference ionic conductivity measured at T_0 ($T_0 = 298$ K), and $\alpha = 0.02\,\text{K}^{-1}$ is the temperature coefficient [29]. We obtained the reference ionic conductivity by:

$$\sigma_0 = \Lambda c, \quad (4)$$

where Λ is the molar conductivity and c is the concentration of the buffer. For 100 mM sodium borate solution, σ_0 is 0.85 S/m. The molar conductivity of an ionic buffer can be estimated by the Onsager's equation:

$$\Lambda = \Lambda^0 - K\sqrt{c} \quad (5)$$

where Λ^0 is the limiting molar conductivity and $K \sim 0.83$ for a 1:1 electrolyte [30]. The limiting molar conductivity for a particular electrolyte can be calculated with the Kholrausch's Law, which states that:

$$\Lambda^0 = \nu_+ \lambda_+^0 + \nu_- \lambda_-^0, \quad (6)$$

where ν_+, ν_- are the stoichiometric coefficients for cations and anions, and the λ^0's are the respective limiting ion conductivity. For sodium borate, we obtained a limiting molar conductivity of 85.3 S cm^2/mol from values of $(\lambda^0)_{\text{sodium}} = 50.10$ S cm^2/mol [29] and $(\lambda^0)_{\text{borate}} = 35.2$ S cm^2/mol [31].

The hydrodynamic problem was treated with the layer model [25]. The mechanical force balance in an electrokinetic system is shown in the Navier–Stokes equation with an electrical force term in Eq. (7) together with the continuity equation.

$$\rho \frac{\partial \boldsymbol{u}}{\partial t} - \nabla \cdot \mu(\nabla \boldsymbol{u} + (\nabla \boldsymbol{u})^T) + \rho(\boldsymbol{u} \cdot \nabla)\boldsymbol{u} + \nabla p + \rho_e \nabla \Phi = 0$$
$$\nabla \cdot \boldsymbol{u} = 0, \quad (7)$$

where ρ_e is the electrical charge density and Φ is the electrical potential. The steady state solution to this equation can be considered as a sum of the inner and outer solutions. The inner solution is the flow within the double layer where viscous and electrical forces dominate, and a no-slip condition is applied at walls. Since the double layer thickness is much smaller than the size of the channel, that is, $\kappa^{-1} \ll \xi$, the flow can be represented by an analytical solution in the direction of the applied field [21]:

$$u_i = \frac{-\varepsilon \zeta}{\mu} \nabla \Phi \quad (8)$$

In the outer region, the inertia forces are important and the electrical forces become negligible if we assume uniform electrical conductivity [25]. Since the outer solution should be continuous with the inner solution, Eq. (9) can be solved numerically to obtain the outer solution using the inner solution as the slip boundary condition (Eq. (10)):

$$-\nabla \cdot \mu(\nabla \boldsymbol{u} + (\nabla \boldsymbol{u})^T) + \rho(\boldsymbol{u} \cdot \nabla)\boldsymbol{u} + \nabla p = 0 \quad \nabla \cdot \boldsymbol{u} = 0 \quad (9)$$

$$u = \frac{-\varepsilon \zeta}{\mu} \nabla \Phi \quad \text{at walls}, \quad (10)$$

where ε is the permittivity, ζ is the buffer zeta potential at the substrate, μ is the viscosity, and Φ is the electrical potential. Both permittivity (7.1×10^{-10} F/m) and viscosity (0.001 Pa s) of water are assumed, and a zeta potential of 0.15 V is used for borosilicate glass [32].

The charge balance inside the channel is described by Ohm's law (Eq. (11)) with the corresponding boundary conditions in Eq. (12), where the walls are assumed to be insulated and the potentials are applied at the two end reservoirs with electrodes.

$$\boldsymbol{i} = -\sigma \nabla \Phi$$
$$\nabla \cdot (-\sigma \nabla \Phi) = 0 \quad (11)$$

$$\begin{aligned} -\sigma\nabla\Phi\cdot\boldsymbol{n} &= 0 \quad \text{at walls} \\ \Phi &= \boldsymbol{V}_i \quad \text{at electrodes} \end{aligned} \tag{12}$$

All calculations were performed with FEMLAB, a finite element simulation and modeling software extension of MATLAB (COMSOL, Burlington, MA, USA). Although recent investigations suggest that two-dimensional hydrodynamic calculations are sufficient to model chip-based electrokinetic systems [33,34], we performed three-dimensional simulations as they are necessary to extract flow behavior inside the finned-structured channels. The heat transfer problems, however, were solved two-dimensionally as field strength is uniform along the straight channel. Note that field distortion typical of a tee or cross-channel injection system [33,35] was omitted in the calculation as these are beyond the scope of the current work.

3. Results and discussion

To better compare the performance of the different geometries and to take into account practical considerations in microfabrication, case studies are subject to the following conditions on the geometry of the cross-section: (1) the total cross-sectional area of all case studies must equal to that of a 500 μm × 275 μm rectangular channel, which serves

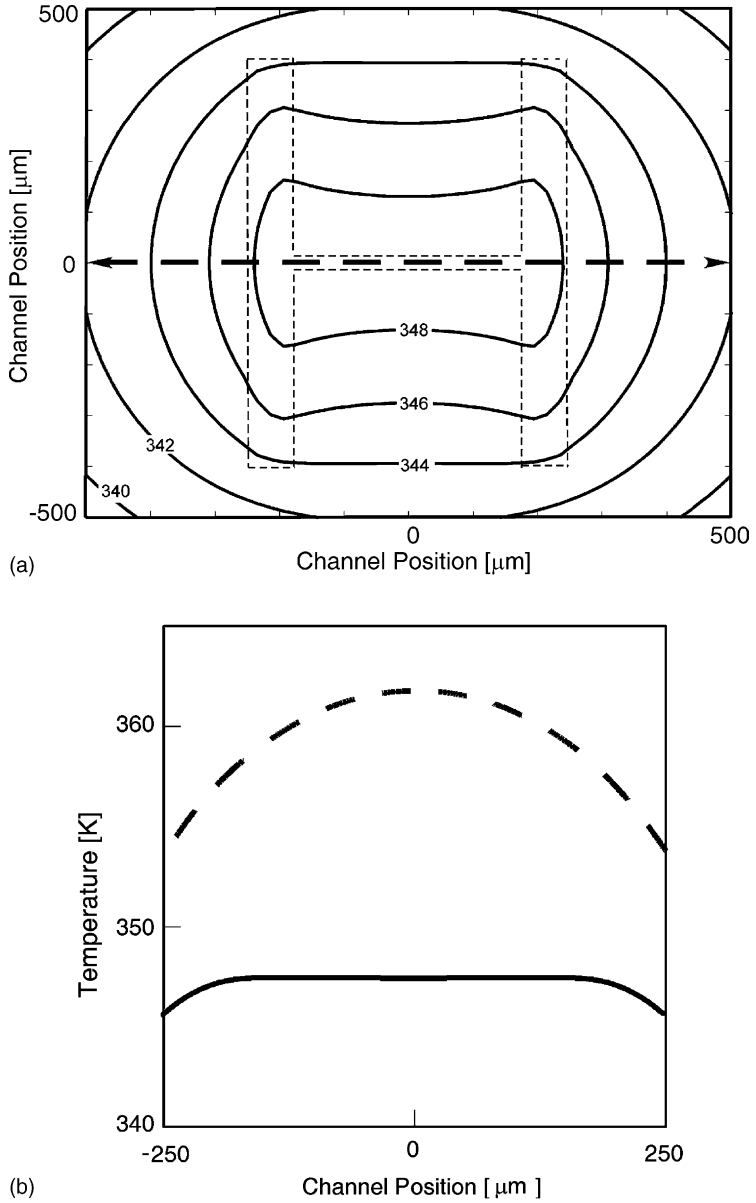

Fig. 2. (a) Contour plot of temperature distribution inside a 4-fin channel; the dashed lines represent the 4-fin channel, and the dashed arrows indicate the location of the centerline; (b) centerline temperature of the 4-fin channel (solid line) compared with that of a bare straight channel (dashed line). The calculation was performed using material properties of glass and an operating condition of 180 V/cm applied to a channel filled with 100 mM sodium borate buffer.

as the basis for comparison, (2) the main channel area (i.e., center of the channel excluding the area of finned extensions) must not exceed 500 μm × 50 μm, which has been determined experimentally to be reliably resistant to inadvertent hydrodynamic flows; and (3) the finned extensions shall not exceed the aspect ratio (height/width) of 5 for ease of microfabrication. Although structures with aspect ratio as high as 20 may be produced with current state-of-the-art technology, they often degrade in replication processes and thus have relatively low yield.

With these three constraints in mind, the first parameter that was investigated is the effect of increased surface area of the channel, which is directly related to the number of finned extensions. Fig. 2a shows the temperature distribution inside a 4-fin channel as isothermal contour lines at identical temperature intervals. Heat is generated inside the buffer by Joule heating and the heat flux that conducts from the channel in the glass substrate is proportional to the temperature gradient, as described by Fourier's law:

$$q = -k\nabla T \tag{13}$$

The convex isothermal lines away from the channel have regular wide spacing, suggesting a relatively gradual flux except at the areas immediately adjacent to the outer boundary of the fins, where the isothermal lines are more compressed. The more compressed lines indicate areas of higher temperature gradient, which implies larger heat flux or more effective heat conduction. In the area bounded by the fins, however, the line spacing is wider and the temperature gradient is more gradual, because this bounded area must absorb and dissipate heat from both the inner boundaries of the fins and the horizontal channel. The centerline temperature inside the 4-fin channel is shown in Fig. 2b and it is compared with that of a bare rectangular 500 μm × 275 μm channel under identical operating conditions. The difference in the two cases is quite apparent: not only does the finned geometry lower the temperature by at least 10 K, the temperature distribution is more uniform across the channel.

Fig. 3a shows the average temperatures of several finned channels with different number of fins. It is evident that the existence of fins in general reduces the temperature, and by at least 12 K when 1–8 fins are used. Fig. 3a also shows the critical field strength, E_c, which is defined as the maximum possible field strength applied to the system while T_{avg} is still below 363 K. E_c serves as a measure for evaluating the operating conditions of this system. In general, when field strength above E_c is applied, a "run-away" operating condition occurs under which excessive current is passed through the buffer solution, resulting in rapid temperature rise, which leads to increases in the ionic conductivity even further because ionic conductivity is a linear function of temperature, which then in turn draws even more current. This is a classic positive-feedback situation that typically ends in rapid vaporization of the buffer solution or devastating electrical arcing through the microchannel. Higher E_c therefore indicates that the system is more robust, or capable of handling

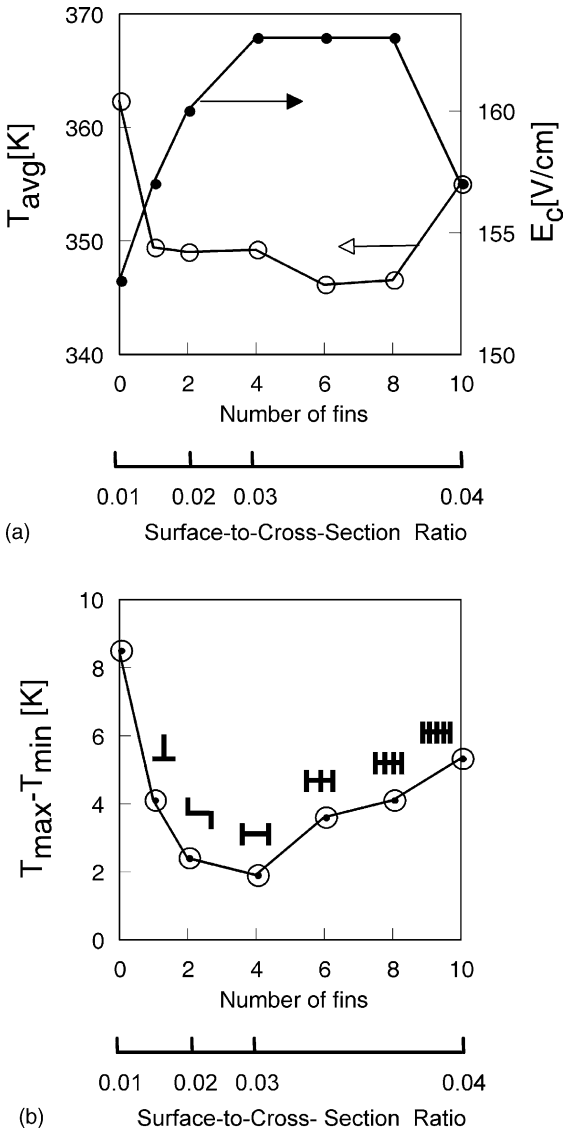

Fig. 3. Characterization of temperature improvement provided by channels having different number of finned surface. (a) Plot of the average inner temperature (open circle) and the critical operating field strength (filled circle) as a function of the number of fins and the surface-to-cross-section ratio. The critical electric field is the maximum field strength that can be applied to the system while the average temperature is still below 363 K. The surface-to-cross-section ratio is defined as the ratio of surface area to volume per unit length of the finned channel. (b) Plot of the maximum temperature change, $T_{max} - T_{min}$, inside the channel as a function of the number of fins and the surface-to-cross-section ratio. The sketches (not drawn to scale) above each data point illustrate the channel cross-sectional geometry of concern. The calculation was performed with field strength of 180 V/cm and using sodium borate buffer at a concentration of 100 mM.

a wider range of operating conditions. The optimum geometry, which corresponds to the lowest temperature rise and the most robust operation, is obtained when 4–8 fins are used.

It is interesting to note that continual increase in the number of fins does not result in better operation from the heat transfer perspective. When 10 fins are used, T_{avg} is higher than that with 8 fins and E_c is reduced. As discussed earlier,

the steepest thermal gradient is adjacent to the outer edges of the outermost fins, where heat conduction is the most effective. The bounded area between the outer fins is not as efficient a heat sink as the rest of the substrate because it must accommodate the heat transferred from three sides, which results in a rise of local temperature and a reduction in the driving force caused by the temperature gradient. In addition, because of the geometric constraints we imposed, the cross sectional area of each fin as well as the bounded area between each pair of fins decreases as the number of fins is increased. Thus, placing additional fins inside the bounded area does not always translate into more efficient heat dissipation. If a material with higher conductivity is used instead of glass (e.g., silicon) or if the distance between the fins is increased, however, the temperature can continue to decrease with a larger number of fins.

Besides increasing interfacial area between the buffer solution and the channel, material choice is another important factor. Polymeric materials have recently been reported as an alternative material for the fabrication of microfluidic devices due to the versatility and ease of fabrication as compared with glass [36,37]. The polymers considered here include: poly(dimethylsiloxane) (PDMS), poly(methyl methacrylate) (PMMA), polycarbonate (PC), and polyester (PET). PMMA has been shown to exhibit significant EOF in native form [38,39]. PDMS exhibits strong EOF after it is oxidized [40], and both PC and PET have been reported to exhibit electroosmotic properties after proper surface treatments [39,41,42]. The choice of substrate material affects only the value of thermal conductivity k_2 used in Eq. (1), since with rapid advances in surface chemistry the EOF properties of various substrates can be controlled and modified [36,37,43].

Fig. 4 shows T_{avg} as a function of the thermal conductivity, calculated using field strengths near E_c and with 100 mM sodium borate as the buffer. The internal temperature of the channel initially decreases precipitously as thermal conductivity of the substrate increases, but when k_2 is >0.28 W/m K the incremental improvement is small. This can be understood by comparing the thermal conductivity of the substrate with that of the buffer solution ($k_1 = 0.60$ W/m K): when substrate thermal conductivity is smaller than that of buffer, temperature rises rapidly as overall heat conduction is reduced. One can compare the limit of low thermal conductivity with the case of adiabatic insulation. However, when substrate conductivity becomes more comparable to that of the buffer, heat removal rate approaches the heat generation rate inside the buffer solution. Beyond this point, increasing substrate conductivity results in diminishing returns in temperature reduction. These results suggest that both glass and polyester are excellent materials to use when only thermal effects are considered. In general, such a finned channel can be constructed by bonding an "upper" section and a "lower" section (divided along the center of the channel), with each section produced by two-layer lithography, that is, the center 500 μm wide portion requires one layer, and the protruding

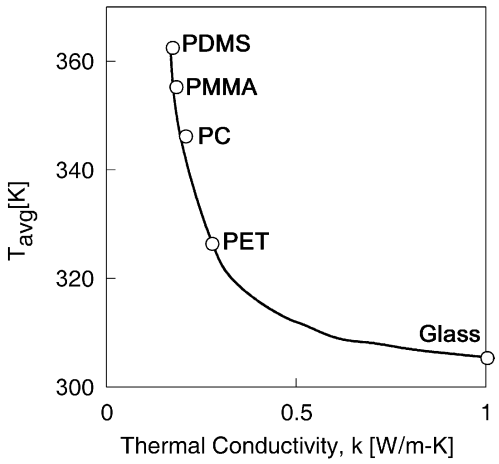

Fig. 4. Plot of the average internal channel temperature inside a 4-fin channel as a function of the thermal conductivity of the substrate under a field strength of 210 V/cm. The materials in consideration (open circle data points) are PDMS (at 0.17 W/m K), PMMA (at 0.18 W/m K), polycarbonate (at 0.205 W/m K), polyester (at 0.275 W/m K) and glass (at 1.0 W/m K). One hundred mM sodium borate buffer was used in the calculation.

fins require a second layer. Current fabrication technique of glass chip is more cumbersome and time-consuming because each prototype would require multiple reactive ion etching steps while that of polyester is relatively simple and cost efficient since rapid replication methods are available.

Besides improvement in heat conduction, the finned surfaces also reduce hydrodynamic effects that may interfere with separation. Recent studies have shown that induced pressure gradient could produce band broadening in electrokinetic flow in capillaries and result in poor CE performance [21,22]. A common source of induced pressure gradients is inadvertent uneven leveling of buffer solution in reservoirs that leads to gravity-driven flow or siphoning. The effect of pressure-driven flow is more pronounced in wide-bore capillaries and can frequently overwhelm the electroosmotic flow. The presence of additional surfaces imposes more no-slip boundary conditions to pressure-driven flow and effectively dampens out the bulk fluid motion. With the increase in surface-to-volume ratio in finned surfaces, flow distortion due to pressure gradient is dampened and re-distributed inside the channel.

Three-dimensional steady state calculations were performed to investigate the hydrodynamic behavior inside preparative scale channels with an equivalent cross section of 275 μm × 500 μm. The channels were assumed to be glass and have a zeta potential of 0.15 V [32]. When no pressure was applied, plug-flow profiles were obtained for all channel designs, in good agreement with expected ideal electroosmotic flow. When a differential pressure of 1.0 mm water height between two reservoirs of a bare rectangular channel was applied, a strong parabolic profile across the centerline of the channel was observed as shown in Fig. 5a. In a 4-fin channel the velocity profile was significantly

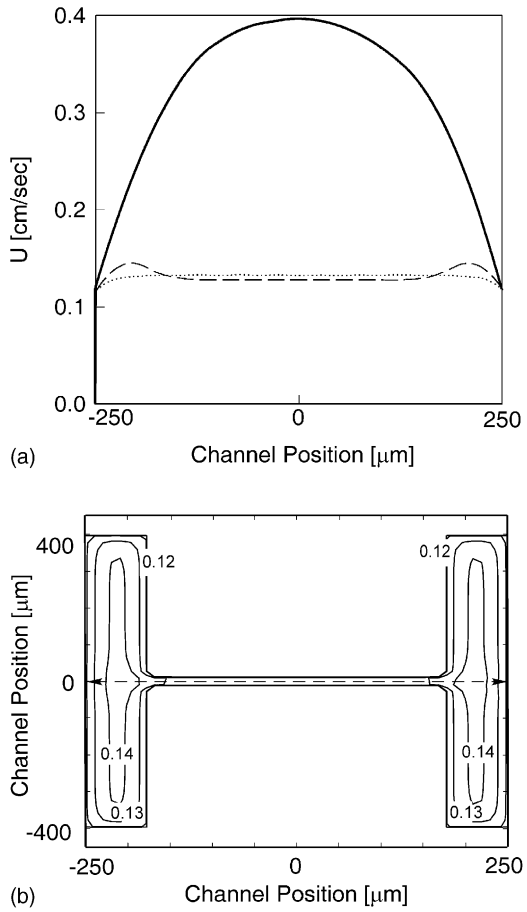

Fig. 5. (a) Centerline velocity profiles of a bare channel (——), 4-fin channel (- - -), and 10-fin channel (· · ·). (b) Contour plot of velocity potential inside a 4-fin channel. In all cases 1.0 mm water (∼10 Pa) was the differential pressure assumed between reservoirs that are 3.0 cm apart. A field strength of 167 V/cm was applied to generate electroosmotic flow.

damped, and it became virtually flat when a 10-fin structure is used. Fig. 5b shows the corresponding velocity contour profile inside a 4-fin channel. Inertia effects produced by the pressure difference were re-distributed among the fins and the main channel. Although there were slight distortions near the fin locations, the effects were much less pronounced in comparison with that of bare rectangular channel.

The separation performance of fin structures can be evaluated by estimating the number of theoretical plates:

$$N = \frac{L^2}{\sigma_T^2}, \tag{14}$$

where L is the typical separation length, and σ_T^2 is the total variance in the peak width due to dispersion. Assuming that all the dispersive processes are independent and random, the total variance can be calculated as the linear combination of these processes [19]:

$$\sigma_T^2 = \sum_j \sigma_j^2 = \sigma_{th}^2 + \sigma_h^2, \tag{15}$$

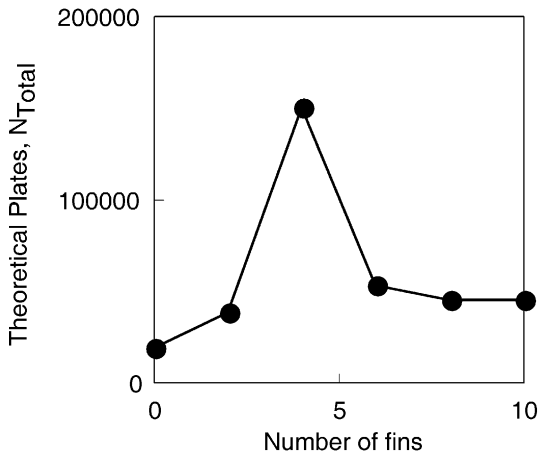

Fig. 6. Plot of the number of theoretical plates vs. the number of fins present. The calculation assumes a 3 cm long channel. Note the number of theoretical plates will be increased in longer channels. The 4-fin geometry, due to the best thermal dissipation, offers the best separation capability.

where σ_{th} refers to deviation from uniform thermal distribution and σ_h refers to deviation from an ideal plug flow. We neglected the contribution caused by longitudinal diffusion because for a typical protein with a diffusion coefficient (D) in water of $\sim 1 \times 10^{-6}$ cm^2/s, the corresponding variance (σ_d^2) is $\sim 2Dt \sim 6 \times 10^{-5}$ cm^2 in our 3 cm long channel and at our flow velocity of 0.1 cm/s, which is much less than our calculated value of $\sigma_T^2 \sim 2 \times 10^{-4}$ cm^2. Fig. 6 shows the performance in separation as a function of the number of fins for a 3 cm long channel. With increased surface area, most fin structures can provide improvement by a factor of 2–3. When a 4-fin design is used, however, a eightfold improvement in performance can be accomplished. This difference in enhancement is primarily due to efficacious thermal management in the 4-fin configuration. Note the number of theoretical plates will increase rapidly with the length of the channel in our calculations because only dispersions caused by thermal and hydrodynamic issues are considered.

4. Conclusion

Based on theoretical and numerical analyses, this paper shows channel topography is an important parameter by which electrokinetically based separation can be dramatically improved, especially in situations where large volumetric throughput is required, such as in preparative or semi-preparative scale operations. Although there have been efforts to scale up CE and CEC, none have been focused on the effect of channel topography in a chip format. With advances in microfabrication, however, the ability to pattern channel morphologies becomes practical. An awareness and understanding of the importance of channel topographies in chemical separations will be critical in advancing this central area of analytical chemistry and in fully exploiting

the capabilities provided by both established and emerging methods in micro- and nano-fabrication.

Acknowledgements

This work was supported by NIH under grant number GM 65293.

References

[1] J.E. Celis, P. Gromov, Curr. Opin. Biotech. 10 (1999) 16.
[2] J.R. Yates, in: Proteomics Workshop at HPCE 2001, Boston, MA, 2001.
[3] M.T.W. Hearn, Adv. Chromatogr. 20 (1982) 1.
[4] M.T.W. Hearn, J. Chromatogr. 418 (1987) 3.
[5] M.T.W. Hearn, A.N. Hodder, M.-I. Aguilar, J. Chromatogr. 327 (1985) 47.
[6] Q.M. Mao, M.T.W. Hearn, Biotechnol. Bioeng. 52 (1996) 204.
[7] C.A. Retamal, P. Thiebaut, E.W. Alves, Anal. Biochem. 268 (1999) 15.
[8] J. Poráth, P. Flodin, Nature 4676 (1959) 1657.
[9] T.C. Laurent, J. Kilander, J. Chromatogr. 14 (1964) 317.
[10] N.P. Golovchenko, I.A. Kataeva, V.K. Akimenko, J. Chromatogr. 591 (1992) 121.
[11] M.C. Wang, L.A. Valenzuela, G.P. Murphy, T.M. Chu, Invest. Urol. 17 (1979) 159.
[12] E. Wen, R. Asiaie, C. Horváth, J. Chromatogr. A 855 (1999) 349.
[13] J.K. Debowski, J. Liq. Chromatogr. Rel. Technol. 25 (2002) 1875.
[14] K.K. Unger, M. Huber, K. Walhagen, T.P. Hennessy, M.T.W. Hearn, Anal. Chem. 74 (2002) 200A.
[15] H.F. Yin, C. Keely-Templin, D. McManigill, J. Chromatogr. A 744 (1996) 45.
[16] J.R. Veraart, C. Gooijer, H. Lingeman, N.H. Velthorst, U.A.Th. Brinkman, Chromatographia 44 (1997) 129.
[17] C. Fujimoto, H. Matsui, H. Sawada, K. Jinno, J. Chromatogr. A 680 (1994) 33.
[18] I.E. Valko, S.P. Porras, M.-L. Riekkola, J. Chromatogr. A 813 (1998) 179.
[19] P.D. Grossman, J.C. Colburn, Capillary Electrophoresis: Theory and Practice, Academic Press, New York, 1992.
[20] M.L. Marina, M. Torre, Talanta 41 (1994) 1411.
[21] J.G. Santiago, Anal. Chem. 73 (2001) 2353.
[22] A.E. Herr, J.I. Molho, J.G. Santiago, M.G. Mungal, T.W. Kenny, M.G. Garguilo, Anal. Chem. 72 (2000) 1053.
[23] M. Poggel, T. Melin, S. Treutlein, Electrophoresis 23 (2002) 2252.
[24] J.-R. Chen, R.N. Zare, E.C. Peters, F. Svec, J.J. Frechet, Anal. Chem. 73 (2001) 1987.
[25] J.M. MacInnes, Chem. Eng. Sci. 57 (2002) 4539.
[26] M.S. Bello, P.G. Righetti, J. Chromatogr. 606 (1992) 95.
[27] M.S. Bello, P.G. Righetti, J. Chromatogr. 606 (1992) 103.
[28] W.A. Gobie, C.F. Ivory, J. Chromatogr. 516 (1990) 191.
[29] L. Coury, Curr. Sep. 18 (1999) 91.
[30] J.O.M. Bockris, A.K.N. Reddy, Modern Electrochemistry: An Introduction to an Interdisciplinary Area, Plenum, New York, 1974.
[31] H. Corti, R. Crovetto, R. Fernandez-Prini, J. Solut. Chem. 9 (1980) 617.
[32] S. Yao, D. Huber, J.C. Mikkelsen, J.G. Santiago, in: Proceeding of IMECE 2001 ASME International Mechanical Engineering Congress and Exposition, ASME, New York, 2001, p. 1.
[33] S.V. Ermakov, S.C. Jacobson, J.M. Ramsey, Anal. Chem. 70 (1998) 4494.
[34] N.A. Patankar, H.H. Hu, Anal. Chem. 70 (1998) 1870.
[35] S.V. Ermakov, S.C. Jacobson, J.M. Ramsey, Anal. Chem. 72 (2000) 3512.
[36] H. Becker, L.E. Locascio, Talanta 56 (2002) 267.
[37] S.A. Soper, S.M. Ford, S. Qi, R.L. McCarley, K. Kelly, M.C. Murphy, Anal. Chem. 72 (2000) 643A.
[38] L.E. Locascio, C.E. Perso, C.S. Lee, J. Chromatogr. A 857 (1999) 275.
[39] G.S. Fiorini, G.D.M. Jeffries, D.S.W. Lim, C.L. Kuyper, D.T. Chiu, Lab Chip 3 (2003) 158.
[40] X.Q. Ren, M. Bachman, C. Sims, G.P. Li, N. Allbritton, J. Chromatogr. B. 762 (2001) 117.
[41] W. Xu, K. Uchiyama, T. Shimosaka, T. Hobo, J. Chromatogr. A 907 (2001) 279.
[42] Y.J. Liu, D. Ganser, A. Schneider, R. Liu, P. Grodzinski, N. Kroutchinina, Anal. Chem. 73 (2001) 4196.
[43] B. Vaidya, S.A. Soper, R.L. McCarley, Analyst 127 (2002) 1289.